Partial Phase Segregation in Strongly Hydrogen-Bonded and Miscible Blends

Bo Zhu,† Yong He,† Naoko Yoshie,‡ Naoki Asakawa,† and Yoshio Inoue*,†

Department of Biomolecular Engineering, Tokyo Institute of Technology, Nagatsuta 4259, Midori-ku, Yokohama 226-8501, Japan, and Institute of Industrial Science, The University of Tokyo, Komaba-4-6-1, Meguro-Ku, Tokyo 153-8505, Japan

Received December 12, 2003; Revised Manuscript Received February 19, 2004

ABSTRACT: The effect of intermolecular hydrogen bonding on the crystallization kinetics and the morphology of poly(ϵ-caprolactone) (PCL)/4,4′-thiodiphenol (TDP) blends with TDP content 0−20 wt % has been investigated by differential scanning calorimetry, polarizing optical microscopy, X-ray measurements, and in situ FT-IR. The equilibrium melting point (T_m^0) of PCL in the PCL/TDP blends decreases with increasing the TDP content, suggesting the miscibility of the blends as expected when strong hydrogen bonding is involved. Following the depression of T_m^0 and the increase of glass transition (as reported in our previous works), the half-time of crystallization and the spherulite growth rate rapidly decrease with increasing TDP content. By small-angle X-ray scattering measurement, obvious extralamellar segregation of TDP was detected, the extent of which increased with increasing TDP content. The inter-spherulite segregation of TDP was also observed by a polarizing optical microscope and FT-IR microscope. For a given composition, the blends crystallized at 40 °C showed a higher extent of inter-spherulite segregation than that crystallized at 30 °C, which indicated that the crystal growth rate plays the dominant role in the morphological formation. With the progress of crystallization, the content of TDP in the inter-spherulite region increased, resulting in a continuous retardation of spherulite growth and a gradient distribution of TDP along the radius. Moreover, the crystallization of PCL component in the blends induced partial phase segregation in the final structure.

Introduction

Recently, we have published several works on the blends of polyesters with a series of low molecular weight dihydric phenols, trying to reveal the relationship between the formation of hydrogen bonds and the solid-state structures and to explain the effects of such low molecular weight compounds on the thermal as well as the mechanical properties of polyesters.[1−3] Among the polyesters investigated by us, poly(ϵ-caprolactone) (PCL) has the highest capability to form strong hydrogen bonds with nearly all dihydric phenols because of its linear flexible molecular chain without any bulky side chains which interfere with the formation of such bonds. 4,4′-Thiodiphenol (TDP) can form the strongest hydrogen bonds with PCL among the dihydric phenols investigated by us. The formation of strong hydrogen bonds between the proton-accepting polyesters and proton-donating dihydric phenols has promised the miscibility between them. On the other hand, the hydrogen bonds have great effects on the thermal properties of polyesters. The glass transition temperature (T_g) of the blend increases, and the melting temperature of polyester is depressed by blending with such dihydric phenols.

In the present paper, we report on a continuation of our study upon these hydrogen-bonded polyester blends. Here, we focus on the restricted crystallization and the morphology of PCL in the blends with TDP. The previous studies on the crystallization kinetics in the miscible polymer blends have revealed that the crystallization behavior and the nucleation mechanisms were quite dependent on the composition of the diluent.[4−6] Little attention was paid on the crystallization of polyesters in the blends with low molecular weight phenol, in which the crystallization of polyester may be restricted by strong hydrogen-bonding interaction with phenol. In the case of PCL/TDP blends, the reduction of chain mobility, the changes in free nucleation energy due to the specific interaction, and further the dilution of PCL by low molecular dihydric phenols will be expected to result in an alteration of the crystallization kinetics of PCL.

Besides the effects on crystallization, the morphology of crystalline proton-accepting polyesters should be affected by blending with a low molecular weight phenol. It is very interesting to detect the segregation of the low molecular weight phenol. Basically, three different types of segregation are possible to occur schematically in the miscible polymer blends with an amorphous component upon crystallization of the crystallizable component, that is, inter-spherulite segregation, inter-fibrillar segregation, and inter-lamellar segregation. The former two and the latter two kinds of segregation can also be described as extra-lamellar and intra-sphreulitic segregation, respectively.[7] Kinetically, there is a competition between the sphreulitic crystal growth rate and diffusion rate of diluents. If the diffusion rate is slower than the crystal growth rate, due to poor molecular mobility of the diluent, the diluent molecules may be trapped inside the inter-lamellar regions before they had a chance to diffuse out.[8,9] Talibuddin et al.[10] have considered the roles of both intermolecular interaction and the T_g value of the diluent on the segregation distance. They concluded that for weakly interacting systems the T_g value of the diluent governs the length scale of segregation. Nevertheless, the T_g value of the diluent no longer plays a

† Tokyo Institute of Technology.
‡ The University of Tokyo.
* To whom all correspondence should be addressed: Tel +81-45-924-5794; Fax +81-45-924-5827; e-mail yinoue@bio.titech.ac.jp.

10.1021/ma035889t CCC: $27.50
Published on Web 04/09/2004

decisive role to control the segregation scale in strongly interacting systems. The presence of strong interactions helps to promote the segregation by depressing the crystal growth rate. The crystal growth rate, and hence the factors that influence it, was suggested to dominate the length scale of diluent segregation.[10] However, still limited attempts have been made to systematically evaluate the proton-accepted polyester blends with low molecular weight phenols. No results about the morphology of such blend systems have been reported, although it is interesting and necessary for understanding the structure−property relationship.

Thus, based on our previous works, in the present investigation, the crystallization kinetics of PCL in the blends with TDP is investigated by differential scanning calorimetry (DSC), polarizing optical microscopy (POM), and in situ FT-IR to elucidate the relationship between the specific interaction and the crystallization behavior of the blends. Further, the segregation of TDP in the blends will be investigated by small angel X-ray scattering (SAXS) and FT-IR measurements.

Experimental Section

Materials. The PCL sample (number-average molecular weight 1.37×10^5; polydispersity index 1.49; Celgreen PH4) was supplied by the courtesy of Daicel Co. (Japan). TDP was purchased from Tokyo Kasei Kogyo Co. (Japan). The polymer sample and the reagent were used as received.

Preparation of Blend Samples. The blend films of PCL with TDP were prepared by casting dioxane solution of blend samples with an appropriate concentration, 10 mg/mL, on the Teflon dishes. The solvent was allowed to evaporate slowly at room temperature, and then the films formed were dried under vacuum at 50 °C for at least 2 weeks. Prior to the physical analysis, the cast sample was first melted at 85 °C for 2 min in order to get rid of the thermal history and solvents residing in the blend. Next, the melted sample was pressed with a pressure 5 MPa for 3 min to ensure compaction. After that, the pressed film was quenched on an iron block in an oven at given temperatures for crystallization of 30 days.

To indicate the different weight content of the blends, the following codes were used: PCLT10, PCLT20, and so on, where the number referred to weight percentage of TDP in the blend, PCLT referred to the PCL/TDP blend, and PCL was appointed to neat PCL.

DSC. The study on the isothermal crystallization kinetics of the blends was carried out on a Perkin-Elmer differential scanning calorimeter (Pyris Diamond). The weight of all samples was between 5 and 6 mg. The temperature and heat flow scales at different heating rates were carefully calibrated using an indium standard with nitrogen as the purge gas. An isothermal temperature program was used to evaluate the effects of hydrogen bonds on PCL crystallization. After melted at 85 °C for 2 min, the sample was quenched to the desired crystallization temperature (T_c) at a rate of 80 °C/min, and the crystallization curves were recorded until the crystallization time is 4 times the half-life $T_{1/2}$. The crystallization kinetics of PCL was analyzed with using the Avrami equation. For overcoming the overheating effects from a high heating rate and a thickening effects from a low heating rate, a medium heating rate of 10 °C/min was used to detect the melting temperature.

POM. An observation of polarizing optical microscopy was performed on an Olympus BX90 polarizing microscope (Olympus Co., Tokyo, Japan) equipped with a video camera. The polymer sample was placed between a microscope glass and a coverslip and heated with a Mettler FP82HT hot stage. The sample was first heated to a temperature of 85 °C and kept for 2 min and then quenched to the desired crystallization temperature.

X-ray Analyses. Wide-angle X-ray diffraction (WAXD) measurements were carried out on a Rigaku RINT-2000 (Rigaku Co., Tokyo, Japan) with a high linearity scintillation counter (slit collimation), working at 40 kV and 200 mA, with Ni-filtered Cu Kα radiation (λ = 0.154 18 nm). Scans were made between Bragg angles of 5−60° at a scanning rate of 1° min^{-1}. Small-angle X-ray scattering (SAXS) measurements were carried out on the same instrument. Scans were made between Bragg angles of 0.1−2.5°. The intensity was registered with every 0.004°, and X-rays were collected for 4 s at each step.

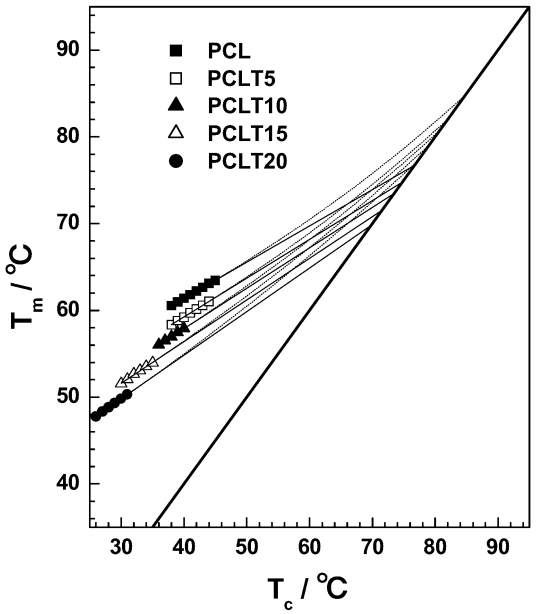

Figure 1. Linear Hoffman−Weeks curves (solid line) and nonlinear M−X plots (dotted line) with an assumption of the lamellar thickening coefficient, γ = 1.5 for PCL and PCL in the PCL/TDP blends.

FT-IR Spectroscopy. FT-IR measurements were carried out on an AIM-8800 (Shimadzu Co., Japan), an automatic infrared microscope. After a sample between two slides of BaF_2 IR window had been melted at 85 °C for 2 min, it was quenched to desired crystallization temperature for FT-IR registration. All the film samples for FT-IR measurements were prepared carefully so that the thickness is thin enough to follow the Beer−Lambert law. A square aperture of 15 × 50 mm was set to register the spectra. All the spectra were recorded at a resolution of 2 cm^{-1} with accumulation of 64 scans.

Results

Equilibrium Melting Points Depression. In our previous works,[1] the NMR data have revealed that the strong hydrogen bonds between the carbonyl groups of PCL and the hydroxyl groups of TDP greatly restrain the mobility of PCL chains. Moreover, the increase of the glass transition temperature of the blends also suggests the reduction of chain mobility with increasing the TDP content. In addition to the effect of hydrogen bonds on the chain mobility of PCL, it should be expected that the specific interaction between the two components could depress the equilibrium melting temperature of PCL, T_m^0. In general, a decrease of chemical potential of polymer systems by an addition of a miscible diluent would result in a decrease of equilibrium melting point. The T_m^0 values of the blends can be determined by plotting T_m against T_c based on the Hoffman−Weeks equation,[11] as shown in Figure 1. The values of T_m^0 are listed in Table 1. The equilibrium melting point of pure PCL is comparable to that reported by Vion et al.[12] From Figure 1 and Table 1, it is clear that the T_m^0 value decreases with the increase of TDP content in the

Table 1. Thermal Properties of PCL/TDP Blends Isothermally Crystallized at 30 °C

sample code	PCL/TDP composition	T_m[a] (°C)	ΔH[b] (mJ/mg)	Φ_c[136 c] (%)	Φ_c[157 d] (%)	$T_m^0{}_{HW}$[e] (°C)	$T_m^0{}_{MX}$[f] (°C)
PCL	100/0	64.6	83.3	59.3	51.0	76.7	84.9
PCLT5	95/5	62.6	77.5	55.0	47.3	74.8	82.1
PCLT10	90/10	60.4	72.3	51.2	44.1	73.5	80.8
PCLT15	85/15	57.7	67.7	47.7	41.1	71.5	79.1
PCLT20	80/20	55.7	57.0	40.0	34.5	69.8	77.2

[a] Melting point (DSC). [b] Melting enthalpy (DSC). [c] Bulk crystallinity with assumption of melting enthalpy for 100% crystalline PCL, 136 mJ/mg. [d] Bulk crystallinity with assumption of melting enthalpy for 100% crystalline PCL, 157 mJ/mg. [e] Equilibrium melting point (linear Hoffman−Weeks plots). [f] Equilibrium melting point (M−X plots with the assumption of $\gamma = 1.5$).

blends. The depression behavior of T_m^0 for the PCL/TDP blends means that the miscibility of the blends is well promised by the formation of the hydrogen bonds between the two components.[13]

Recently, the validity of the linear Hoffman−Weeks extrapolation for the determination of T_m^0 of polymers has been critically reviewed by Marand et al.[14,15] Their results indicated that, first, the linear extrapolation is not justified on theoretical grounds, as it was shown to hold only at exceedingly low supercoolings, which are not experimentally accessible; second, the linear extrapolation leads to an underestimation of the equilibrium melting temperature and an overestimation of the thickening coefficient. The principal reason for this is due to the treatment of the experimentally observed supercooling ($\Delta T = T_m^0 - T_c$) dependence of the initial lamellar thickness, $l^* = C_1/\Delta T + C_2$, where C_1 is equal to $2\sigma_e T/\Delta H_f$ (σ_e is the surface free energy associated with the crystal basal plane, and ΔH_f is the thermal dynamic heat of fusion) and C_2 is a constant accounting for both the term δl (δl is the thickness increment above the minimum lamellar thickness, which enables the secondary surface nucleus to enter a region of thermal dynamic stability at the fastest rate at the temperature of crystallization) and the temperature dependence of the kinetic fold surface free energy, σ_{ex}, obtained experimentally. The C_2 value is always ignored in the classical Hoffman−Weeks linear extrapolation. In that, the linear Hoffman−Weeks extrapolation is only valid at very small supercoolings, where the crystallization would not occur on any practical time scale. It has been argued that the observed melting temperature must vary nonlinearly with the crystallization temperature while C_2 cannot be ignored. Marand et al. suggested that a nonlinear Hoffman−Weeks extrapolation gives more accurate T_m^0 values.[14,15] By plotting $M = T_m^0/(T_m^0 - T_m)$ against $X = T_m^0/(T_m^0 - T_c)$ for different choices of T_m^0, the most optimum T_m^0 value can be obtained, while the slope of M vs X plots is equal to a constant lamellar thickening coefficient, γ. In this study, for comparison, the nonlinear extrapolation has been employed to detect the T_m^0. The lamellar thickening coefficient, γ, is simply assumed to be 1.5. Following the fitting procedures for the $M-X$ plots as described above, it is found the values of T_m^0 based on the $M-X$ plots are indeed much higher than those from the linear Hoffman−Weeks extrapolation, as shown in Table 1. Of course, the assignment of the value of thickening coefficients to 1.5 is unreasonable. However, in this study, the detection of exact values of T_m^0 of PCL and its blends with TDP is beyond the scope of this research. The depression of T_m^0 for PCL in the blends with TDP is more concerned. It is clear that the depression of T_m^0 for PCL in the blends with TDP is similar, no matter what kind of extrapolation method is used.

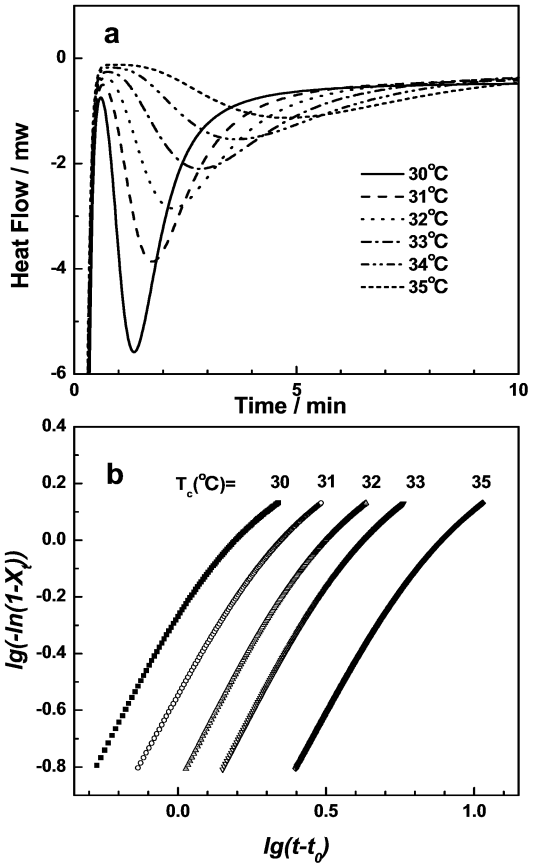

Figure 2. (a) Isothermal crystallization traces of PCLT15. (b) Linear Avrami plots for isothermal crystallization of PCLT15.

Overall Crystallization Rate. The crystallization kinetics of the blends is analyzed by DSC using an isothermal temperature program introduced in the Experimental Section. The overall time dependence of the crystallization is analyzed using the Avrami equation, which relates the crystallinity, X_t, to time, $t - t_0$, by

$$\log[-\ln(1 - X_t)] = n \log(t - t_0) + \log K \qquad (1)$$

where X_t is the ratio of crystallinity at a given time t to the final crystallinity, which was calculated as the ratio of peak area at time t to that at time $t \to \infty$, $\Delta H_t/\Delta H_\infty$, and normalized so as to take unity at $t \to \infty$. K and n are the isothermal crystallization parameter and the Avrami exponent, respectively; t_0 represents the induction period determined experimentally, which is defined as the time where the onset of crystallization occurs in the isothermal crystallization curves, as shown in Figure 2a. In Figure 2b are shown the typical Avrami plots for the PCLT15 blend. Each line shows an initial linear portion and subsequently tends to level off. The

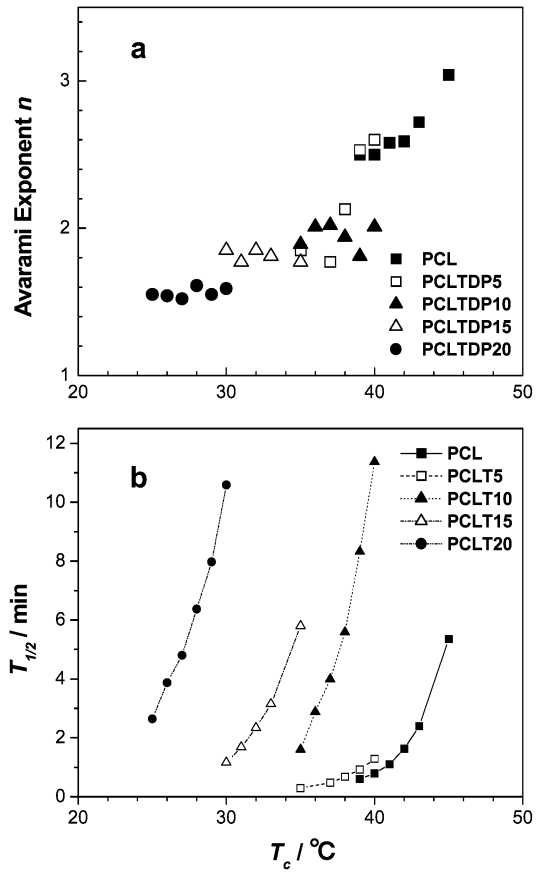

Figure 3. (a) Plots of half-time of PCL crystallization ($T_{1/2}$) vs crystallization temperature (T_c) in the PCL/TDP blends. (b) Plots of Avrami exponent (n) vs crystallization temperature (T_c) in PCL/TDP blends.

initial linear behavior and subsequent leveling off deviation are characteristic of many materials and semicrystalline polymers, including homopolymers, which is normally due to the secondary crystallization caused by the sphreulitic impingement. Besides this reason, the partial segregation of TDP molecules from the intra-spherulitic region into the extra-spherulitic region may partly contribute to such leveling off phenomenon, which will be described in the next section. The extra-spherulitic segregation results to increase the TDP content in the extra-spherulitic phase. Thus, the glass transition temperature increases, and the equilibrium melting point is depressed, which would bring about a deeper restraint on the crystallization of PCL component.

In Figure 3a is shown the value of Avrami exponent n plotted against T_c for pure PCL and the blends with various compositions, determined from the initial linear portion in the Avrami plots. For pure PCL, n ranges from 2.5 to 3.0. For the PCL/TDP blends, the value of n decreases from about 2.5 to 1.5 with TDP content increasing to 20%. As is well-known, the Avrami exponent derived from isothermal crystallization reflects the nucleation and growth dimension of the crystals. Thus, the introduction of TDP seems to disturb the nucleation of PCL in the blends. Keith et al. observed an Avrami exponent of $n = 0.5$ for diffusion-controlled crystallization in system containing high concentration of amorphous diluent.[16,17] In the PCL/TDP blends, not only the dilution but also the strong interaction between the two components would restrain the diffusion of PCL component, which may lead to a lower value of the Avrami exponent. For brevity's sake, the values of K are not shown here. The values of K decrease with increasing TDP content and the crystallization temperature. Since the value of K quite depends on the value of n, we intend to discuss the effects of hydrogen bonds on the crystallization kinetics of PCL component based on the analysis of half-life $T_{1/2}$ instead of that of K.

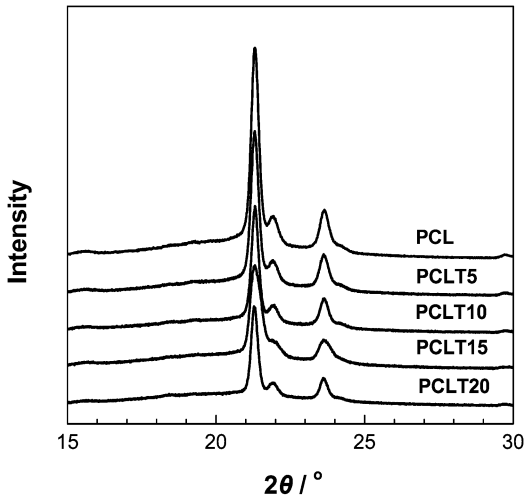

Figure 4. X-ray diffraction patterns of PCL/TDP blends with different TDP weight content.

In Figure 3b are shown the values of the half-life $T_{1/2}$ plotted against the crystallization temperature for PCL and its blends with TDP, where $T_{1/2}$ is the time when the crystallinity reaches 0.5. The data collected at only lower degree of supercooling are shown because at higher degree of supercooling, the isothermal crystallization of PCL in the pure state and the blends starts before reaching the thermal equilibrium in the DSC sample room. It is well-known that crystallization behavior of polymers is mainly governed by a nucleation process and its molecular mobility. The overall crystallization rate is controlled by a nucleation process at lower degree of supercooling and controlled by a diffusion process at higher degree of supercooling. For the hydrogen-bonded PCL/TDP blends, however, the crystallization process is somewhat more complex. The overall crystallization rate of PCL in the blends was reduced not only by the PCL dilution but also by the chemical potential changes of the liquid phase due to the formation of strong hydrogen bonds between the two components in the liquid phase. This interaction will alter the free energy necessary for forming a critical nucleus on the surface of crystallizable component and the mobility of two components. As can be seen in Figure 3, the half-life $T_{1/2}$ of the PCL component is affected so much by the blend composition. When the TDP content in the blends increase to just 10%, the half-life $T_{1/2}$ of the PCL component shows large change from 0.8 to 11.4 min, indicating that the specific interaction between PCL and TDP greatly restrains the crystallization of PCL component.

Lamellar Morphology. Because the crystallization is extremely slow in the blends containing less than 75 wt % PCL, we primarily focus on the blends containing no more than 20 wt % TDP. Figure 4 shows the typical X-ray diffraction patterns of the PCL/TDP blends with TDP content from 0 to 20 wt % crystallized at 30 °C. It is clear that only one crystalline structure, the same as that of PCL lattice, is observed for the neat polymer and the blends. The melting behavior was also measured for

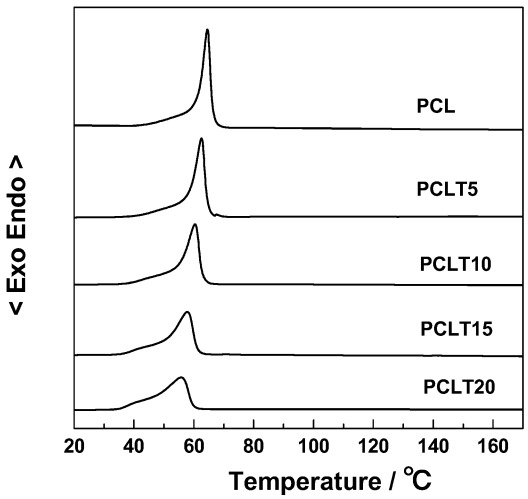

Figure 5. DSC heating traces of PCL/TDP blends isothermally crystallized at 30 °C.

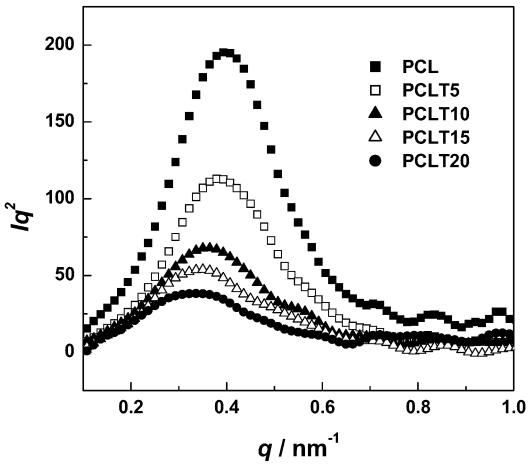

Figure 6. Lorentz-corrected SAXS intensities of PCL/TDP blends isothermally crystallized at 30 °C.

these samples by using DSC at a heating speed of 10 °C/min, as shown in Figure 5. It is very clear that only one endothermic peak, belonging to the melting behavior of PCL, is observed. No melting point corresponding to TDP is found in these thermograms (a melting point of pure TDP is 160 °C).[2] Thus, only PCL component is crystallized in the blends within the composition range investigated here, while TDP is unable to crystallize due to the formation of strong hydrogen bonds with PCL. So, these blends with TDP content less than 25% can be assumed to be the crystalline/amorphous blend systems. Employing the two-phase model, the lamellar morphology is analyzed on the basis of SAXS measurements.

For a crystalline/amorphous blend, clarification of the location of the amorphous component in the microphase is important, as it affects the properties of the blends distinctively. In the present study, the morphological structure of the PCL/TDP blends is probed by SAXS. Figure 6 shows the profiles of Lorentz-corrected intensity (Iq^2) of the semicrystalline PCL/TDP blends crystallized at 30 °C. The peak position (q_{max}) shifts toward small angle with increasing TDP content, showing that the long period (L) calculated on the basis of Bragg's law increases. In the lamellar stack model with sharp phase boundary, the long period represents the sum of the crystal thickness (L_c) and the amorphous layer thickness (L_a). Thus, the increase of the long period may

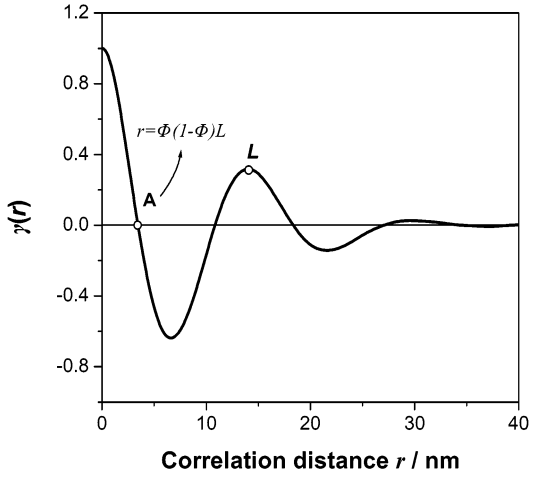

Figure 7. Graphical representation of one-dimensional correlation functions for neat PCL isothermally crystallized at 30 °C.

thus stem from the thickening of PCL crystals or the swelling of amorphous layers upon blending with TDP. From SAXS profiles, the average long period, the average amorphous thickness, and the average crystal thickness can be calculated by specific methods. One of more precise ways is to use the one-dimensional correlation function $\gamma(r)$, which is obtained directly from the intensities smeared by a slit of infinite height,[18] as defined by

$$\gamma(r) = \{\int_0^\infty sI(s)[J_0(2\pi rs) - 2\pi rsJ_1(2\pi rs)]\,ds\}/\{\int_0^\infty sI(s)\,ds\} \quad (2)$$

where r is the direction along which the electron density is measured, $s = 2 \sin \theta/\lambda$, and J_n is a Bessel function of order n. As the correlation function is related to the intensity function by the Fourier transformation, one may calculate the morphological parameters from direct graphical analysis of the correlation function. Figure 7 displays an inverse Fourier transform to the scattering relation for the experimental scattering profiles. Before the inverse Fourier transformation, the subtraction of thermal background, extrapolation to $S = 0$ by using Guinuier's law,[19] and extrapolation to ∞ through the application of Porod's law[20−22] should be carried out. The first maximum in $\gamma(r)$ corresponds to the long period L. Assuming the corresponding two-phase model, L_c and L_a can be measured via simple geometric analysis of $\gamma(r)$.[23] The thickness of the thinner layer L_1 is given by the intersection between the straight line extrapolated from the self-correlation triangle and the baseline. However, this approach is not correct when the amorphous and the crystalline layer thickness distribution do overlap. Normally, the overlap of the amorphous and the crystalline layer thickness distribution would not bring a flat first minimum in the $\gamma(r)$, which is the case as shown in Figure 7.

Hence, an alternative method is used here, using the so-called quadratic expression.[24] As shown in Figure 7, the intersection of the linear regression of the self-correlation triangle with the abscissa always occurs at $r = \Phi(1 - \Phi)L$, where Φ and $1 - \Phi$ are the volume fractions of the phases in the semicrystalline stacks. This intersection is sometimes labeled "A", and the expression is known as the quadratic expression, which represents a second method to calculate the morphologi-

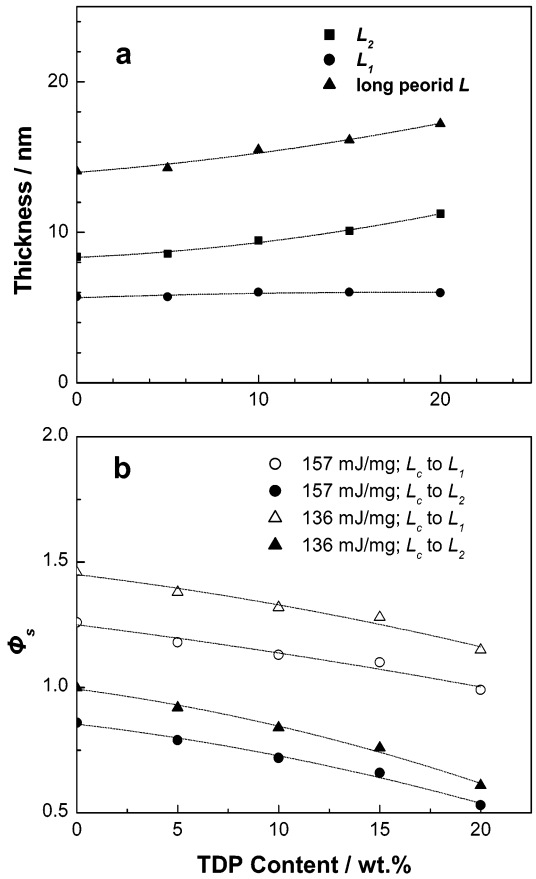

Figure 8. (a) TDP content dependence of the average long period (L) and the average thinner thickness (L_1) and the average thicker thickness (L_2) for PCL/TDP blends isothermally crystallized at 30 °C. (b) TDP content dependence of the volume fraction of lamellar stacks (Φ_s) for PCL/TDP blends isothermally crystallized at 30 °C (157/136 mJ/mg: Φ_s is calculated with employing 157/136 mJ/mg as the melting enthalpy of 100% crystalline PCL; L_c to L_1/L_2: L_c is assigned to L_1/L_2).

cal parameters. As the quadratic nature of the expression, it yields two possible solutions for Φ, that is, one solution Φ with a value below 0.5, and the other solution $1 - \Phi$ with a value above 0.5. So, the thickness of the thinner layer is $L_1 = L\Phi$, while that of the thicker one is then given by $L_2 = L - L\Phi$. Figure 8a presents the detailed lamellar parameters calculated with the one-dimensional correlation function for neat PCL and the PCL/TDP blends isothermally crystallized at 30 °C. The value of L_1 increases distinctively while that of L_2 increases slightly with the TDP content.

When the linear crystallinity, Φ_c^{lin}, is smaller than 0.5, L_1 is L_c and L_2 corresponds to L_a. The reverse is true for $\Phi_c^{lin} > 0.5$. The linear crystallinity is defined as

$$\Phi_c^{lin} = L_c/L = L_c/(L_c + L_a) \tag{3}$$

Provided that the spherulites are volume filling, Φ_c^{lin} is related to the bulk crystallinity Φ_c by

$$\Phi_c = \Phi_s \Phi_c^{lin} \tag{4}$$

where Φ_s is the volume fraction of lamellar stacks in the sample. If the whole volume is homogeneously filled with lamellar stacks, $\Phi_s = 1$ and $\Phi_c^{lin} = \Phi_c$; if the sample is not homogeneously filled, $\Phi_s < 1$ and $\Phi_c^{lin} > \Phi_c$.

Thus, the assignment of the crystal thickness (L_c) to L_1 or to L_2 has to be made on the basis of determination of the bulk crystallinity by other techniques, such as DSC measurements. Normally, the mass crystallinity can be calculated from the melting enthalpy of the PCL component (the area of the DSC melting peak in the first heating scan), with measurement of the melting enthalpy (ΔH^0) of 100% crystalline PCL. Unfortunately, three values of ΔH^0 for PCL, 157, 167, and 136 mJ/mg, have been reported by the ATHAS databank, Lebedev,[25] and Grescenzi,[26,27] respectively. It has led to a controversy in the analysis on lamellar morphology of PCL, as the crystal thickness L_c may be attributed to the shorter (L_1) with adopting the highest value, while to the larger (L_2) length with adopting the lowest value. However, based on their own choice of ΔH^0 for PCL, a series of studies have still been devoted to describe the morphological behavior of PCL and its blends. In some cases, the crystal thickness was attributed to the thicker length (L_2)[28−31] because of its higher value of crystallinity than 50% and in others to the thinner length (L_1) with its lower value of crystallinity than 50%.[32,33]

For comparison, two values of ΔH^0 for PCL, 157 and 136 mJ/mg, are used to calculate the bulk crystallinity, Φ_c^{136} and Φ_c^{157}, respectively, for the blend samples used for SAXS measurements, as shown in Table 1. (The bulk crystallinity of the blends, Φ_c, is calculated from the mass crystallinity measured by DSC with taking account of the density difference between the crystal and amorphous layer.) For neat PCL, its Φ_c^{136} far above 50% make it reasonable to assign the thicker length as the crystal thickness, while its Φ_c^{157} very close to 50% makes the assignment less straightforward. Thus, in this research, the assignment of crystal thickness also seems to quite depend on the choice of ΔH^0 for PCL. Moreover, it is sure that the different assignments of crystal thickness may lead to a different conclusion on the segregation behavior of TDP in blends. To evaluate the effect of assignments on the description of phase behavior in the PCL/TDP blends, both the assignment of crystal thickness to the larger length (L_2) and to the shorter length (L_1) are employed in spite of the value for the bulk crystallinity. Moreover, based on the assignments, the volume fractions of lamellar stacks (Φ_s) corresponding to different choice of ΔH^0 for PCL are calculated with employing eqs 3 and 4. In Figure 8b, the values of Φ_ss are plotted against the TDP composition. Fortunately, with both assignments, the values of Φ_ss decrease with increasing the TDP content. That is, the tendency for variation of Φ_ss with the TDP content is independent of the assignments and the choice of ΔH^0 values. As is well-known, the magnitude of Φ_s can be closely related to the morphological structures, and larger extent of extra-lamellar segregation will result in smaller Φ_s. Thus, the dependence of Φ_s on the TDP content suggests TDP can segregate to extra-lamellar region, and the extent of extra-lamellar segregation rises with the TDP content. However, it should be noted that Φ_s with value above 1 has no physical significance, since the value of Φ_s for the sample homogeneously filled with lamellar stacks is only 1.

Spherulite Morphology. The kinetics of sphreulitic growth in the PCL/TDP blends was investigated here. It is observed that the spherulitic growth rate decreases with the TDP content in the blends (data are not shown here). This depression in kinetics should be attributed

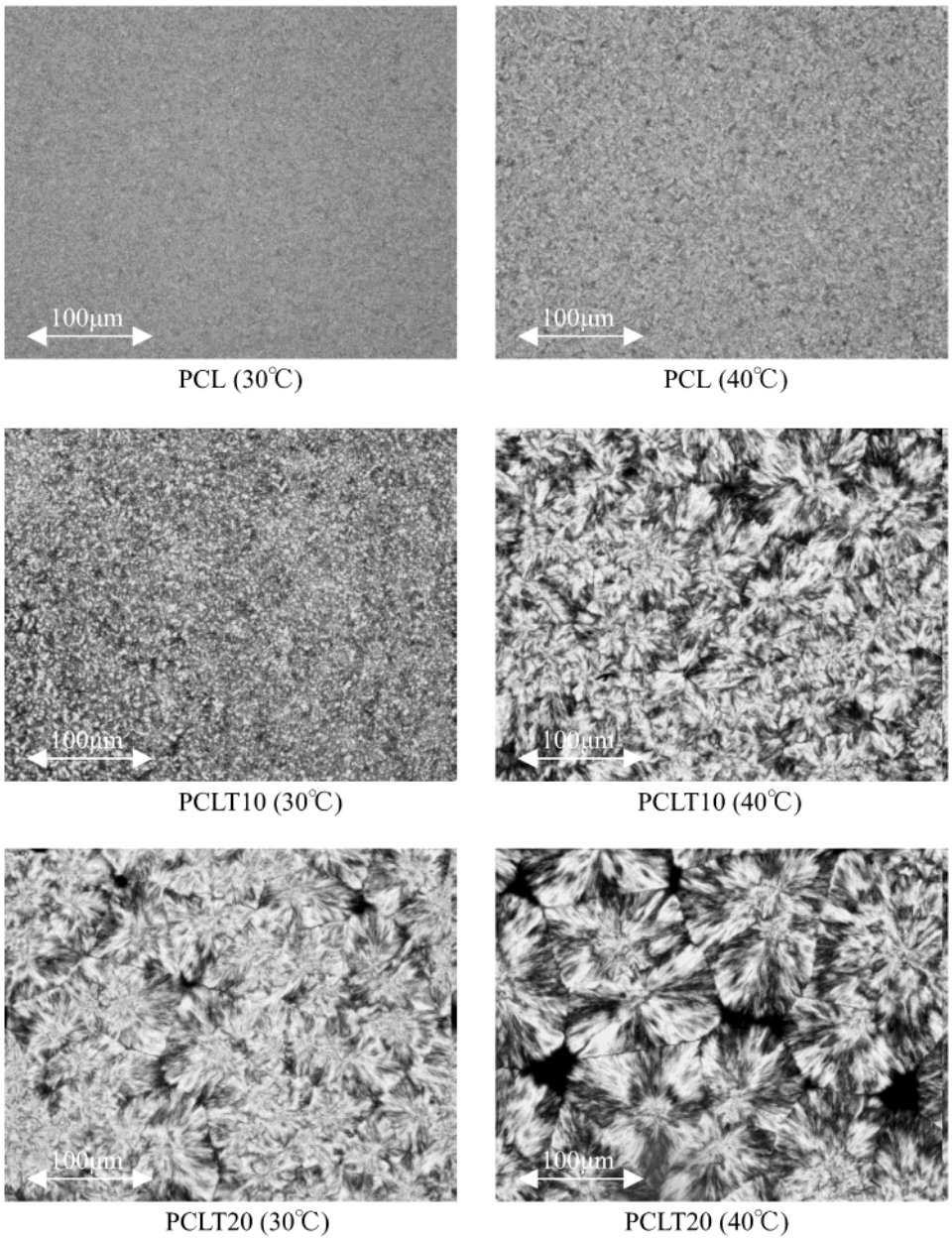

Figure 9. Polarizing optical microscopic photographs for PCL/TDP blends with various TDP content isothermally crystallized at 30 and 40 °C.

to the reduction of chain mobility (because of the T_g increase), the dilution of the PCL component at the growth front, and the change in free energy of nucleation (due to the specific interaction). It is also noted that the time dependence spherulite growth is nonlinear, which should be related to the exclusion of TDP from the spherulite. It will be discussed in detail later.

As described in above section, the SAXS data indicated that a part of TDP segregates into the extralamellar region, but it was not clear whether TDP can segregate into the inter-spherulite or not. In Figure 9 are shown the polarized optical micrographs of PCL and the PCL/TDP blends grown at 30 and 40 °C. Compared with the volume-filled morphology of pure PCL, the blends show partially filled morphology, which indicates the segregation of TDP from the intra-spherulite region. The partially filled morphology of spherulites is quite consistent with their nonlinear growth kinetics. The inter-spherulite segregation is the result of the competitive rate processes, that is, the growth of PCL crystal and the diffusion of TDP molecule. The depressed growth of PCL crystal results in the segregation of TDP from the inter-fibrillar region into the inter-spherulite region.

By comparing the morphology of samples crystallized at 40 °C with those crystallized at 30 °C, as shown in Figure 9, it is reasonable to find that the amorphous phases separated by spherulites in the blends crystallized at 40 °C are larger than those crystallized at 30 °C, in that the growth rate decreases with the increase of the crystallization temperature in the low supercooling range (nucleation-controlled). Thus, at 40 °C, more TDP can diffuse into the inter-spherulite region than at 30 °C. As a result, the area of uncrystalline phase increases, as shown in Figure 9.

It is also noted that the segregation of proton-donating diluent in the PCL/TDP blends is quite deeper than that in other similar hydrogen-bonding polyester blend systems with proton-donating polymer, such as poly(3-hydroxybutyrate)/poly(vinylphenol) (PVPh),[34] PCL/

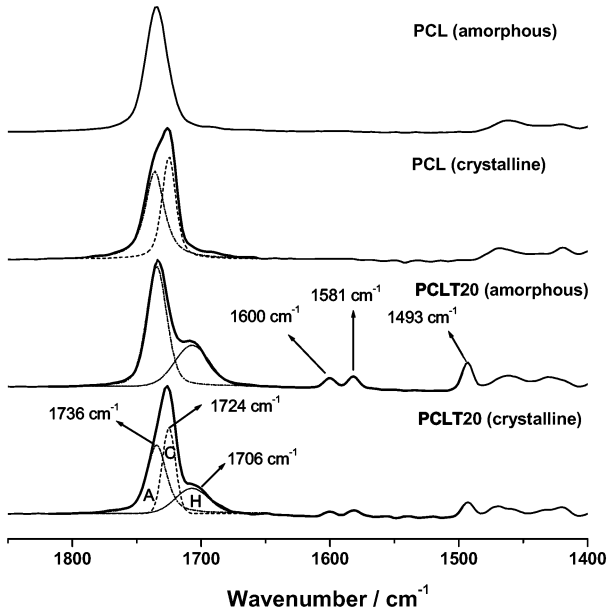

Figure 10. FT-IR spectra measured at 40 °C for the PCL (amorphous) and the PCLT20 (amorphous), obtained upon quenching from melting, and the PCLT20 after crystallized for 10 h. A: amorphous carbonyl component; C: crystalline carbonyl component; H: hydrogen-bonded carbonyl component.

PVPh,[31] and poly(L-lactide)/PVPh blends.[35] The different segregation level may result from the different extent of restriction of the crystallization by the hydrogen bonds. In addition, as the diffusion rate of low molecular weight compound is faster than that of macromolecules, it can be expected that the deeper segregation should occur in the PCL/TDP blends.

In Situ Observation of the Segregation during Crystallization. It is suggested by the SAXS and POM data that, during the crystallization of PCL component in the blends, TDP can segregate from the inter-lamellar to the inter-spherulite region. However, the arguments on the phenomenon are not very clear yet. Thus, a FT-IR microscope is used here for in situ observation of the TDP segregation by detecting the TDP content change in a certain region of the blends during the crystallization process. Since PCLT20 has a slow crystallization rate and can be obtained as the amorphous state upon quenching, it would be a very good candidate for the in situ observation by FT-IR. The area of the square aperture for FT-IR registration is $15 \times 50\ \mu m^2$, which is much smaller than the area of PCL spherulites (about $\pi 70^2\ \mu m^2$) in the blend. The PCL and PCLT20 are quenched from the melt to 40 °C for crystallization. When the temperature of sample get to 40 °C, the measurement of FT-IR was started. The induction time of crystallization for PCL and PCLT20 at 40 °C is so long that the spectra for PCL and PCLT20 sample in the amorphous state can be registered in time. In Figure 10 are shown the FT-IR spectra registered at 40 °C for a crystalline PCL, amorphous PCL, amorphous PCLT20, and crystalline PCLT20 sample. Comparing the spectrum of amorphous PCLT20 with that of amorphous PCL, it is clear that the PCLT20 sample shows three peaks located at 1493, 1581, and 1600 cm^{-1}, which cannot been found for the plain PCL sample. These peaks are denoted to the C=C vibration of TDP. In both the spectra of PCL and PCLT20, there is a distinctive C=O vibration absorption. In this study, the C=C vibration absorption, located at 1493 and 1581 cm^{-1}, and the C=O vibration absorption are used to quantitatively analyze the TDP content in a certain region with a area of $15 \times 50\ \mu m^2$.

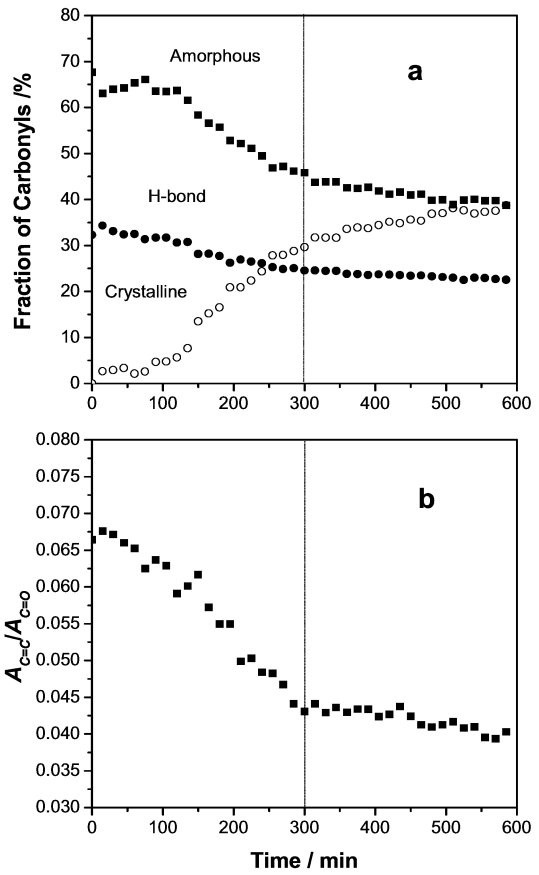

Figure 11. (a) Time dependence of the amorphous, crystalline, and hydrogen-bonded carbonyl components in PCLT20 during the crystallization process. (b) Time dependence of the vibration absorbance ratio of C=C to C=O vibration during the crystallization process.

As well-known, the basis for any quantitative analysis of spectroscopy is the Beer−Lambert law relating the absorbance A to the path length b and the concentration c with the proportionality constant a as $A = abc$. So the concentration of TDP, C_{TDP}, can be related to that of PCL, C_{PCL}, by the ratio of the absorbance of C=C vibration to that of C=O vibration as $C_{TDP}/C_{PCL} = A_{C=C}/A_{C=O}$. On the basis of our previous research,[2] the integrated absorbance of the carbonyl vibration band can be resolved into at least three components, that is, the amorphous, $A_{(a,CO)}$, the crystalline, $A_{(c,CO)}$, and the hydrogen-bonded, $A_{(b,CO)}$, as shown in Figure 10. In Figure 11 are shown the time dependence of the amorphous, crystalline, and hydrogen-bonded carbonyl components in PCLT20 during the crystallization process. It is quite clear that the sample at the beginning of measurement is in the amorphous state, since the crystalline carbonyl component cannot be detected. With the time elapsing, the fraction of crystalline carbonyls increases, while those of hydrogen-bonded and amorphous carbonyls decrease. Moreover, based on the results of curve resolving analysis, the integrated absorbance of the carbonyl vibration band can be calculated as $A_{CO} = A_{a,CO} + \gamma_{a/bAb,CO} + \gamma_{a/cAc,CO}$, where $\gamma_{a/b}$ (0.51) and $\gamma_{a/c}$ (0.68)[1,2] are the absorption coefficients which take into account the difference among the absorptivities of the amorphous, hydrogen-bonded, and crystalline carbonyl components.

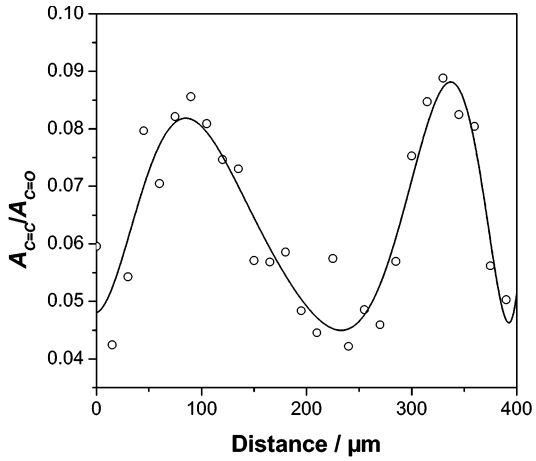

Figure 12. Ratio of the absorbance of C═C vibration to that of C═O vibration plotted against the distance from the center of the spherulite along the radial direction observed for the PCLT20 blend after crystallization at 40 for 15 h.

Following the procedure introduced above, the ratio of the absorbance of C═C vibration to that of C═O vibration can be calculated. In Figure 11b is shown the change of absorbance ratio during the crystallization of PCLT20. Distinctively, the ratio decreased with the crystallization elapsing, indicating that the TDP content in the limited area reduced; that is, TDP segregated out from the blend. The results accord well with those of SAXS and POM measurements. Besides the dynamic detection of the TDP segregation, FT-IR is also used to measure the TDP contents at different position in the spherulites of the PCLT20 blend. With comparing the spatial difference in the TDP content, the path for the TDP segregation can be speculated. In Figure 12, the ratio of the absorbance of C═C vibration to that of C═O vibration was plotted against the distance from the arbitrary selected center of the spherulite along the radial growth direction in the PCLT20 blend after 15 h crystallization at 40 °C. As expected, the TDP content at various places in the spherulite is very different. That is, the TDP content increases along the radial direction. However, the TDP content does not always increase but decrease when it passes a maximum value at about 80 μm, which is just the spherulite radius in the blends, indicating the segregation of TDP continuously increases along the radius of spherulite. With the crystallization, TDP segregates from the intra-spherulite region into the inter-spherulite region, as observed by the in situ FT-IR measurement. The increase of TDP content in the inter-spherulite region would lead to an increase of T_g and a decrease of T_m^0. In turn, a continuous retardation of spherulite growth and a distribution of TDP along the radius direction can be observed as expected. That is, the TDP content at the center of the spherulite is the lowest, and the TDP content increases along the radius of the spherulite. As shown in Figure 12, the minimum value corresponds to the center of the spherulite, while the maximum corresponds to the edge of the spherulite. It indicates that the TDP content increases along the radius from the center to the edge of the spherulite.

Discussion

Some authors have suggested that the mobility of the amorphous component is a key parameter determining the segregation level.[8,9,36] However, for the strongly interacting systems, the growth rate of crystal lamellar was suggested to control the segregation level rather than the mobility.[10] For the blend system investigated in this study, the crystallization of the PCL component is restricted by the strong hydrogen-bonding interaction with TDP. That is, the higher value of T_g and lower degree of supercooling, as detected by DSC, depress the crystallization of PCL component in the blends with TDP. Therefore, the decreasing growth rate of the lamellar should give TDP molecules enough time to diffuse into the inter-fibrillar region and even deeper inter-spherulite region despite the strong hydrogen-bonding interaction between the two components.

With the progress of the crystallization, the content of TDP in the inter-spherulite region increased, followed by the increase of T_g and the decrease of T_m^0. In return, a continuous retardation of spherulite growth and a distribution of TDP along the radius direction can occur, as evidenced by Figures 11 and 12. When the content of TDP becomes high enough, the spherulites cannot grow anymore, resulting in the existence of inter-spherulite amorphous phase, as shown in Figure 9. Taking into account the distribution of TDP along the radius direction, it can be expected that the TDP content in the inter-spherulite region should be higher than that in the inter-fibrillar region.

Also, the distribution of TDP along the radius direction should lead to a distribution of the lamellar thickness along the radius. As detected by SAXS, both L_1 and L_2 increase with increasing the TDP content. Similarly, for an individual crystal, its thickness also should depend on the local TDP content around its growing front. Thus, the crystal becomes thicker along the radius. The extent of distribution of crystal thickness caused by the TDP segregation indirectly evidenced by the fact that the isothermally crystallized blends show wider melting peak than pure PCL during the DSC heating scan, as shown in Figure 5. It also seems that the distribution of crystal thickness broadens with increasing the TDP content in the blends, as the melting peak broadens. However, besides the effects of hydrogen bonds on the crystal thickness, changes in the melting enthalpy or crystal perfection should not be negligible. The changes in the melting enthalpy or crystal perfection along with segregation of TDP would also broaden the melting peak.

The segregation of TDP may result in the different TDP content among the inter-lamellar, the inter-fibrillar, and the inter-spherulite region. That is, the crystallization of PCL may induce partial phase segregation in the final structure. In Figure 13 is shown the heating DSC curves of the PCL/TDP blends isothermally crystallized at 40 °C. It is clear that all blend samples show three distinct thermal transition behaviors, although the two ones at higher temperature are very weak. They are designated as T^L, T^M, and T^H from low to high of temperature transitions. All these temperatures increase with TDP content in the blends. Clearly, the thermal transition behavior of T^L should correspond to a glass transition. For T^M and T^H, there are two possible explanations, that is, the glass transitions of various locations and the cold crystallizations. It seems more possible that T^M and T^H arise from the glass transitions of various locations, as the segregation of TDP results in different distributions of TDP content at various locations. As discussed above, the TDP content in the inter-spherulite region should be higher than that in

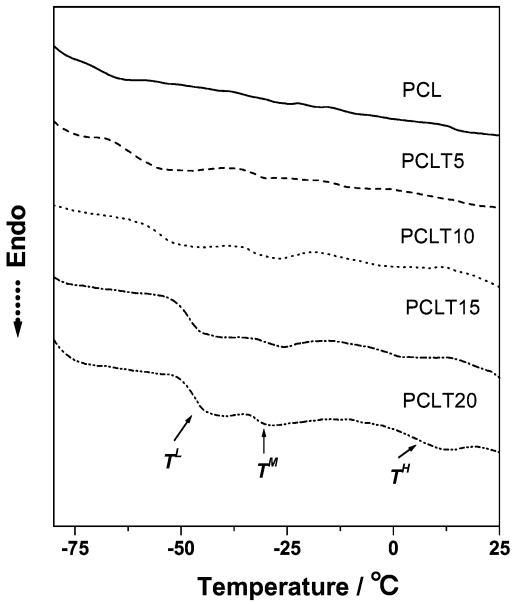

Figure 13. Multi-T_g behavior of the PCL/TDP blends isothermally crystallized at 40 °C.

the inter-fibrillar region. Thus, T^M may correspond to the inter-fibrillar region while T^H to the inter-spherulite region. Another possibility is that T^M and T^H may come from the cold-crystallization of PCL component in the inter-fibrillar and inter-spherulite region, where the higher content of TDP would like to restrict the crystallizations of PCL very much. However, regardless of the assignments of T^M and T^H to glass transitions or cold crystallizations, both of them should be in response to the partial phase separation.

Conclusion

In this article, the effects of hydrogen-bonding interaction on the crystallization kinetics and phase morphology have been investigated for the PCL blends with diphenol TDP. The FT-IR spectra as well as the depression of the equilibrium melting point of PCL indicated the formation of strong intermolecular hydrogen bonds between PCL and TDP. The crystallization of PCL in the blends with TDP was restricted by the formation of very strong hydrogen bonds. As detected by SAXS and POM, it is found that the TDP molecules in the interlamellar region can segregate through the inter-fibrillar region until into the inter-spherulite region. With the aid of in situ FT-IR, the segregation kinetic of TDP from the intra-spherulite into the inter-spherulite region has been measured. Further, it was found that, in the final state of the PCL/TDP blend, the TDP content decreases with the distance from the center of the spherulite along the radius of the spherulite. Moreover, the crystallization of PCL component in the blends likely induces partial phase segregation in the final structure.

Acknowledgment. The authors thank Daicel Co. (Tokyo, Japan) for the kind gift of PCL sample. This work was partially supported by a Grant-in-Aid for Scientific (A), No. 14208104 (2003), from the Ministry of Education, Science, Sports, and Culture (Japan).

References and Notes

(1) He, Y.; Asakawa, N.; Inoue, Y. *Macromol. Chem. Phys.* **2001**, *202* 1035.
(2) He, Y.; Asakawa, N.; Inoue, Y. *J. Polym. Sci., Part B: Polym. Phys.* **2000**, *38*, 1848.
(3) Li, J.; He, Y.; Inoue, Y. *J. Polym. Sci., Part B: Polym. Phys.* **2001**, *39*, 2108.
(4) Wang, Z.; Jiang, B. *Macromolecules* **1997**, *30*, 6223.
(5) Rahman, M. H.; Nandi, A. K. *Polymer* **2002**, *43*, 6863.
(6) Pedrosa, P.; Pomposo, J. A.; Calahorra, E.; Cortazar, M. *Polymer* **1995**, *36*, 389.
(7) Huo, P. P.; Cebe, P.; Capel, M. *Macromolecules* **1993**, *26*, 4275.
(8) Defieuw, G.; Groeninckx, G.; Reynaers, H. *Polym. Commun.* **1989**, *30*, 267.
(9) Debier, D.; Jonas, A.; Legras, R. *J. Polym. Sci., Polym. Phys. Ed.* **1998**, *36*, 2197.
(10) Talibuddin, S.; Wu, L.; Runt, J.; Lin, J. S. *Macromolecules* **1996**, *29*, 7527.
(11) Hoffman, J. D.; Weeks, J. J. *J. Res. Natl. Bur. Stand.* **1962**, *66A*, 13.
(12) Vion, J. M.; J'erome, R.; Teyssie', P.; Aubin, M.; Prud'homme, R. E. *Macromolecules* **1986**, *8*, 451.
(13) Qin, C.; Pires, A. T. N.; Belfiore, L. A. *Polym. Commun.* **1990**, *31*, 177.
(14) Marand, H.; Xu, J.; Srinivas, S. *Macromolecules* **1998**, *31*, 8219.
(15) Xu, J.; Srinivas, S.; Marand, H. *Macromolecules* **1998**, *31*, 8230.
(16) Keith, H. D.; Padden, F. J. *J. Appl. Phys.* **1964**, *35*, 1270.
(17) Keith, H. D.; Padden, F. J. *J. Appl. Phys.* **1964**, *35*, 1286.
(18) Balta-Calleja, F. J.; Vonk, C. G. In *X-ray Scattering of Synthetic Polymers*; Elsevier: Tokyo, 1989.
(19) Guinier, A.; Fournet, G. In *Small-Angle Scattering of X-rays*; John Wiley & Sons: New York, 1955.
(20) Porod, G. *Kolloid-Z.* **1951**, *124*, 83.
(21) Porod, G. *Kolloid-Z.* **1952**, *125*, 51.
(22) Porod, G. *Kolloid-Z.* **1952**, *125*, 108.
(23) Strobl, G. R.; Schneider, M. *J. Polym. Sci., Polym. Phys. Ed.* **1980**, *18*, 1343.
(24) Goderis, B.; Reynaers, H.; Koch, M. H. J.; Mathot, V. B. F. *J. Polym. Sci., Polym. Phys. Ed.* **1999**, *37*, 1715.
(25) Lebedev, B.; Yevstropov, A. *Makromol. Chem.* **1984**, *185*, 1235.
(26) Crescenzi, V.; Manzini, G.; Calzolari, G.; Borri, C. *Eur. Polym. J.* **1972**, *8*, 449.
(27) Khambatta, F. B.; Warner, F.; Russel, T.; Stein, R. S. *J. Polym. Sci., Polym. Phys. Ed.* **1976**, *14*, 1391.
(28) Russell, T. P.; Stein, R. S. *J. Polym. Sci., Polym. Phys. Ed.* **1983**, *21*, 999.
(29) Vanneste, M.; Groeninckx, G.; Reynaers, H. *Polymer* **1997**, *38*, 4407.
(30) Kuo, S.; Chan, S.; Chang, F. *J. Polym. Sci., Polym. Phys. Ed.* **2004**, *42*, 117.
(31) Chen, H.; Wang, S.; Lin, T. *Macromolecules* **1998**, *31*, 8924.
(32) Heck, B.; Hugel, T.; Iijima, M.; Sadiku, E.; Strobl, G. *New J. Phys.* **1999**, *1*, 17.
(33) Men, Y.; Strobl, G. *Macromolecules* **2003**, *36*, 1889.
(34) Xing, P.; Dong, L.; An, Y.; Feng, Z. *Macromolecules* **1997**, *30*, 2726.
(35) Chen, H.; Liu, H.; Lin, J. *Macromolecules* **2000**, *33*, 4856.
(36) Defleuw, G.; Groenincks, G.; Reynaers, H. *Polymer* **1989**, *30*, 267.

MA035889T